metals

MDPI

Article

The Effects of Straw-Returning Processes on the Formation of Fe-Mn (Hydr)oxide Colloids and Arsenic Bioavailability

Junhao Zheng [1], Mei Jiang [1], Qingzhu Li [1,2], Zhihui Yang [1,2], Qi Liao [1,2], Mengying Si [1,2] and Weichun Yang [1,2,*]

[1] School of Metallurgy and Environment, Central South University, Changsha 410083, China; 203501048@csu.edu.cn (J.Z.); 233512175@csu.edu.cn (M.J.); qingzhuli@csu.edu.cn (Q.L.); yangzh@csu.edu.cn (Z.Y.); liaoqi@csu.edu.cn (Q.L.); simysmile@csu.edu.cn (M.S.)

[2] Chinese National Engineering Research Center for Control & Treatment of Heavy Metal Pollution, Changsha 410083, China

* Correspondence: yang220@csu.edu.cn

Abstract: The objective of this study was to investigate the effect of straw return on the formation of Fe-Mn colloids in arsenic-contaminated soils and its subsequent influence on arsenic behavior. It was observed that organic matter (SD) resulting from straw decomposition interacted with iron/manganese (hydr)oxides (Fe/Mn (hydr)oxides) present in the soil, leading to the formation of colloidal particles. These particles significantly influenced the fixation and release of arsenic. The experimental results indicated that an increase in SD content facilitated the formation of colloidal particles. The highest concentration of colloidal particles was observed at a C/Fe-Mn ratio of 2.2, which significantly reduced the bioavailability and mobility of arsenic in the soil. The increase in SD content also diminished the depositional attachment efficiency of SD/Fe-Mn, thereby enhancing its migration through the soil. The actual field soil-filled column experiments further demonstrated that the content of SD significantly influenced arsenic bioavailability and mobility. Specifically, at a C/Fe-Mn ratio of 2.2, the inhibition of arsenic migration and bioavailability was found to be 1.46 times more effective compared to a C/Fe-Mn ratio of 0.4. Therefore, the return of straw to the field represents an effective soil remediation strategy for mitigating the bioavailability of arsenic by modulating the C/Fe-Mn ratio. This approach offers a novel perspective on strategies for heavy metal remediation.

Keywords: Fe/Mn (hydr)oxides; straw-derived; arsenic; migration

Citation: Zheng, J.; Jiang, M.; Li, Q.; Yang, Z.; Liao, Q.; Si, M.; Yang, W. The Effects of Straw-Returning Processes on the Formation of Fe-Mn (Hydr)oxide Colloids and Arsenic Bioavailability. *Metals* **2024**, *14*, 1289. https://doi.org/10.3390/met14111289

Academic Editor: Antonije Onjia

Received: 18 October 2024
Revised: 8 November 2024
Accepted: 11 November 2024
Published: 14 November 2024

1. Introduction

Arsenic (As) contamination in paddy fields has emerged as a significant global concern due to its severe implications for human health [1,2]. The primary sources of As in rice-growing soils include irrigation with As-contaminated groundwater, the application of As-containing pesticides, and mining activities [3,4]. This As can undergo various transport and transformation processes, enabling its absorption by plants and subsequent entry into the food chain through rice, which serves as a staple food for over half of the world's population [5]. Consequently, this leads to chronic exposure that triggers health issues such as skin damage, cardiovascular diseases, and cancer [6–8]. In light of the widespread prevalence of As contamination and its serious repercussions, there is an urgent need to develop effective strategies for managing and mitigating As pollution in paddy fields.

As a globally recognized agricultural practice, straw return is not only advocated as a primary method for straw management but also acknowledged for its beneficial effects on soil enhancement [9,10]. Soluble organic matter derived from straw (SD) contains functional groups such as carboxyl groups (-COOH) and phenolic hydroxyl groups (-OH) [11,12]. These functional groups can form stable complexes with heavy metals, thereby reducing their adsorption and increasing the mobility of heavy metals (e.g., As, Pb, etc.) in soil [13–15]. However, the phenomenon of reduced heavy metal accumulation

in plants is observed in practical applications of straw return [16–18]. This effect may be attributed to the formation of complex colloids between dissolved organic matter (DOM) generated from straw and Fe/Mn (hydr)oxides present in the soil, which facilitates the stabilization of As [19]. Further research has demonstrated that in the combined presence of dissolved DOM and Fe/Mn (hydr)oxides, arsenic exists in multiple forms, as follows: partially dissolved in solution, partially complexed with DOM within the aqueous phase, and partially encapsulated within small colloids. In aqueous environments, the concentrations of arsenic and dissolved DOM exhibit similar patterns [20]. Specifically, arsenic demonstrates a correlation with DOM concentrations and affects its transport and distribution in the environment by binding to colloids that are rich in both DOM and Fe as well as Mn [21,22]. Therefore, a comprehensive investigation into the transport processes of SD and the complex colloids formed by Fe/Mn (hydr)oxides during straw incorporation into soil is crucial for understanding their influence on arsenic behavior. This knowledge is essential for mitigating As contamination in rice fields.

In this study, we aim to address the existing knowledge gap by thoroughly investigating the mechanisms involved in the colloid formation of straw-derived (SD) materials and Fe/Mn (hydr)oxides, as well as the complex processes of migration and deposition. A key focus of this research is the molar ratio of carbon to iron/manganese (C/Fe-Mn), which is proposed as a critical factor influencing the formation and transport of SD-Fe/Mn colloidal particles. By elucidating these mechanisms, this investigation seeks to enhance our understanding of As dynamics within paddy soil while providing novel insights for innovative soil remediation strategies.

2. Materials and Methods

2.1. Materials

Straw was sourced from dry rice fields in Changsha County, Hunan Province, China. Prior to utilization, the straw underwent air-drying and was ground through a 60-mesh sieve. Straw-derived suspensions were prepared by immersing the straw in 500 mL of ultrapure water at a temperature of 368 K under dark conditions. Subsequently, the pH was adjusted to 10.5 using a 1 Mmol/L NaOH solution, and the resulting solutions were filtered through a cellulose nitrate filter with a pore size of 0.45 μm. To determine the concentration of organic matter derived from straw (SD), a standard curve relating dilution degree to organic carbon content was established through a concentration gradient experiment, with the results presented in Figure S1. The organic carbon (C) content in the SD stock solution was measured multiple times using a total organic carbon (TOC) analyzer (Multi N/C 3100, Jena Analytics, Jena, Germany), yielding an average result of 963.8 ± 5.9 mg C/L (n = 4). This stock suspension was subsequently utilized to prepare suspensions at various working concentrations for further experiments [23,24]. The fluorescence excitation–emission matrix (EEM) spectra of SD suspensions were recorded using a fluorescence spectrophotometer (Hitachi F-7000, Hitachi, Tokyo, Japan). The excitation wavelengths ranged from 250 to 500 nm, while the emission wavelengths spanned from 200 to 400 nm, with intervals of 5 nm. The resulting fluorescence spectra for each component are presented in Figure S2. Based on the positions of the EEM, as well as the EEM profiles and spectral loadings, two fluorescent components were identified (Table 1). The identified components included complex amino acids and protein-like substances corresponding to Peak I, along with a variety of aromatic proteins exhibiting a strong specific fluorescence intensity associated with Peak II [25,26].

Table 1. Range distribution of fluorescence area integrals for SD.

	Area	Ex (nm)	Em (nm)	Type
SD	I	220–320	250–350	Soluble microbial byproduct-like
	II	205–225	275–350	Aromatic protein

Note: Before EEM measurements, dilute samples with UV absorbance over 0.1 at 254 nm using milli-Q water to reduce internal filtering effects.

The experimental soil was sampled in May 2022 in the paddy field area of Yiyang City, Hunan Province. Soil samples were collected using methods consistent with previous studies [27]. The concentration of decarbonate-extracted bioavailable As was determined to be 23.1 ± 0.75 mg/kg. Detailed information regarding the physicochemical properties of the soil, including dissolved organic carbon (DOC), cation exchange capacity (CEC), and decarbonate-extracted bioavailable As concentrations, is provided in Table S1.

Phytic acid (H_2SO_4, 99%), nitric acid (HNO_3, 70%), hydrochloric acid (HCl, 36%), sodium hydroxide (NaOH), sodium bicarbonate ($NaHCO_3$), ferrous sulfate ($FeSO_4 \cdot 7H_2O$), and calcium chloride ($CaCl_2$) were commercially available from Sinopharm Chemical Reagent Co., Ltd. (Shanghai, China). Magnesium chloride ($MgCl_2$) and sodium chloride (NaCl) were purchased from Shanghai Macklin Biochemical Technology Co., Ltd. (Shanghai, China). Potassium permanganate ($KMnO_4$) was sourced from Xilong Scientific Co., Ltd. (Guangzhou, China). All the reagent solutions were prepared using ultrapure water with a resistivity greater than 18 MΩ·cm, obtained from Milli-Q systems by Millipore in Shanghai, China. With the exception of straw, all chemicals utilized in this study were of analytical grade.

2.2. Formation and Characterization of SD-Fe/Mn Colloids

To elucidate the impact of the carbon-to-iron/manganese (C/Fe-Mn) molar ratio on the formation of SD-Fe/Mn colloids, a series of batch experiments were conducted. Stock solutions containing SD with concentrations ranging from 0 to 50 mg of carbon per liter of ultrapure water (C/L) were prepared. Subsequently, specific amounts of $FeSO_4 \cdot 7H_2O$ and $KMnO_4$ solutions, each at a concentration of 10 mg/L, were added to achieve mixtures with C/Fe-Mn molar ratios varying from 0 to 21.5. In this context, the term C/Fe-Mn refers to the ratio of the relative molar mass of organic carbon to the combined relative molar masses of iron and manganese. The detailed process for material preparation is illustrated in Figure 1. These molar ratios were selected as they encompass a range commonly observed in sediment samples [23,28,29]. The pH of the system was carefully maintained at 7.0 ± 0.1 using 5 mM NaOH. The suspensions underwent stirring at a rate of 400 rpm at room temperature for a duration of 12 h to facilitate the production of SD-Fe/Mn (hydr)oxide colloids. Detailed information regarding the experimental conditions is provided in Table S2.

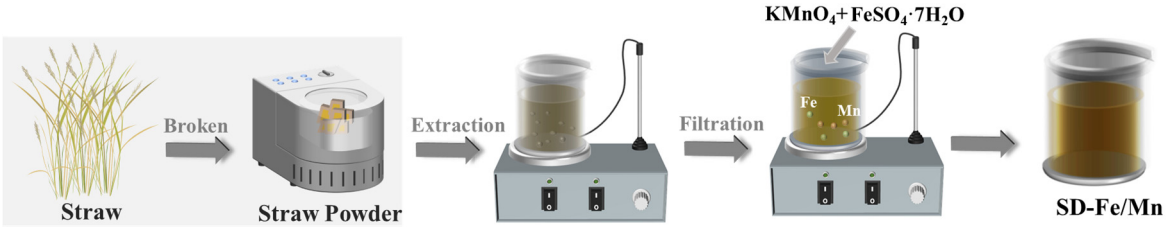

Figure 1. Synthesis process of SD-Fe/Mn.

The concentration of SD, Fe, and Mn in the colloidal samples was analyzed as follows according to size fractionation: dissolved species (<1–3 nm), colloidal particles (1–3 nm to 450 nm), and particulate (>450 nm) [30]. The total Fe/Mn (hydr)oxide concentration in each fraction was determined by inductively coupled plasma mass spectrometry (ICP-MS) (NEXION 2000, Perkin Elmer, Waltham, MA, USA), following the acidification of samples with 2% HNO_3. Dynamic light scattering (DLS) was conducted using a Zetasizer Nano (NanoBrook Omni, Brookhaven, NY, USA) to evaluate the particle size distribution and zeta potential of the NOM-Fe/Mn suspensions [24]. Transmission electron microscopy (Talos F200X, Thermo Fisher, Waltham, MA, USA) was utilized to examine the morphology of the resulting colloids. Colloidal samples were prepared by depositing approximately 20 μL of colloidal suspension onto a 200-mesh carbon-coated copper grid, followed by the evaporation of residual water under vacuum at room temperature. Solid colloids were

isolated via ultracentrifugation and subsequently freeze-dried. The resulting sample was characterized using Attenuated Total Reflection Fourier Transform Infrared Spectroscopy (ATR-FTIR) (Nicolet iS50, Thermo Fisher, WLM, USA) to analyze the functional groups present. The rationale for employing the ATR method is its minimal impact on the sample, thereby ensuring a non-destructive analysis.

2.3. Colloid Deposition Kinetics

A dissipative quartz crystal microbalance (QCM-D) (Analyzer, Biolin, GBG, SWE), equipped with four flow cells, was employed to evaluate the deposition of SD-Fe/Mn colloids on the silica interface. The silica surface was chosen as the model surface due to its representation of a significant environmental surface exhibiting properties akin to quartz sand. The deposition experiments were performed according to the previous literature [31]. Briefly, a background solution was introduced into the chamber to establish a baseline until the mean normalized third overtone frequency shift no longer exceeded 0.5 Hz and stabilization of the baseline occurred for 10 min. Subsequently, SD-Fe/Mn colloidal suspensions with varying C/Fe/Mn molar ratios but identical electrolyte compositions were injected into the sensor for a duration of 20 min. The frequency change (Δf) and energy dissipation (ΔD) of the QCM-D crystal coated with silica (5 MHz) were monitored simultaneously [32,33]. Further details regarding the experimental procedure can be found in Text S2.

2.4. Column Experiments

The migration of SD-Fe/Mn colloids in packed quartz sand columns was investigated by column experiments. Quartz sand was used to simulate the soil environment [34,35], and its migration in soil was examined by constructing soil-filled columns with a porosity of 27.2 ± 0.2%, comparable to that used in As migration experiments [36], as detailed in Text S1. The flow chart for the specific soil-filled column experiment is shown in Figure 2.

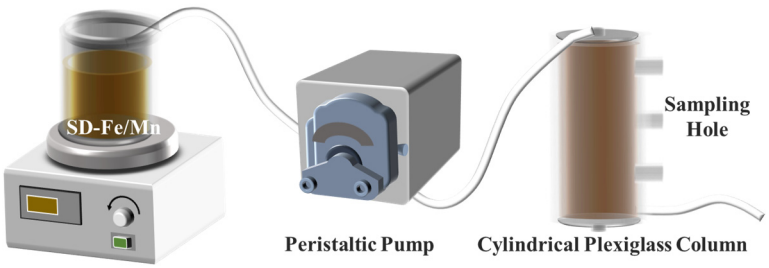

Figure 2. Flowchart of the soil-filled column experiment.

To assess the impact of SD-Fe/Mn colloids on As mobility in soil, Yiyang farmland soil was utilized within circular Plexiglas columns. Approximately 395 g of soil was packed into the Plexiglas cylinders (inner diameter 3.5 cm × length 15 cm), resulting in a soil porosity of 26.9%. A peristaltic pump controlled the injection flow rate, allowing for the continuous introduction of five pore volumes (PV) of agitated SD-Fe/Mn colloid into each column from top to bottom at a Darcy flow rate of 2.93 m/day. After seven days, each column medium was divided into three layers measuring 4–5 cm each; these were carefully excavated using gravity techniques for sand grain analysis. Each layer was further subdivided into thirds based on inner diameter segments measuring between 1.1 and 1.2 cm. Naturally air-dried measurements were conducted to determine the chemical compositional distribution of As within the samples. A total of 1.0 g of air-dried soil samples was weighed into a 50 mL centrifuge tube, followed by the addition of 10 mL deionized water for water-soluble extraction and $NaHCO_3$ at a solid–liquid ratio of 1:10 g/mL for decarbonate-extracted bioavailability assessment. The sample mixture underwent shaking for two hours at a speed of 180 r/min at room temperature (25 ± 2 °C). Subsequently, this extracted bioavailable fraction underwent additional shaking under identical conditions before being filtered. Post

filtration, atomic fluorescence spectrometry (AFS) (HGF-V2, Haiguang, CN) determined the concentration levels of decarbonate-extracted bioavailable As present in the reacted soils.

2.5. Quality Control and Data Analysis

All containers utilized in the experiments were immersed in a 10% HNO_3 solution for 24 h, followed by triple rinsing with deionized water prior to the commencement of the experiments. Standard reference materials were employed to calibrate instruments and validate analytical measurements related to the physicochemical properties and heavy metal analysis of the soils. Replicate experiments were conducted to ensure consistent results and account for any experimental variability. Data processing was performed using Excel 2021 and SPSS 19.0, with results expressed as mean value ± standard deviation (±SD). The coefficient of variation among triplicate analyses remained within 5% for the studied heavy metals and associated properties. Origin 2023 was utilized for data fitting, graph plotting, and further processing.

3. Results

3.1. Morphological Distribution of SD-Fe/Mn Colloids

The influence of the C/Fe-Mn molar ratio on the distribution of SD-Fe/Mn fractions was examined by analyzing the percentages of each morphology (dissolved species, colloidal particles, and particulate) of SD and Fe/Mn (hydr)oxides in the SD-Fe/Mn suspensions. The results are presented in Figure 3. The results indicated that the fractions of dissolved species and colloidal particles of organic carbon in SD-Fe/Mn suspensions exhibited a relatively stable distribution, with approximately 90% of SD existing as colloidal particles (Figure 3a). However, irrespective of the molar ratio of C/Fe-Mn, a fraction of the dissolved species SD remained in a dissolved state and did not form colloidal complexes with Fe/Mn (hydr)oxides. This phenomenon may be attributed to the fact that the surfaces of the dissolved species SD were in a relative equilibrium state, rendering them unable to bind effectively to Fe/Mn (hydr)oxides.

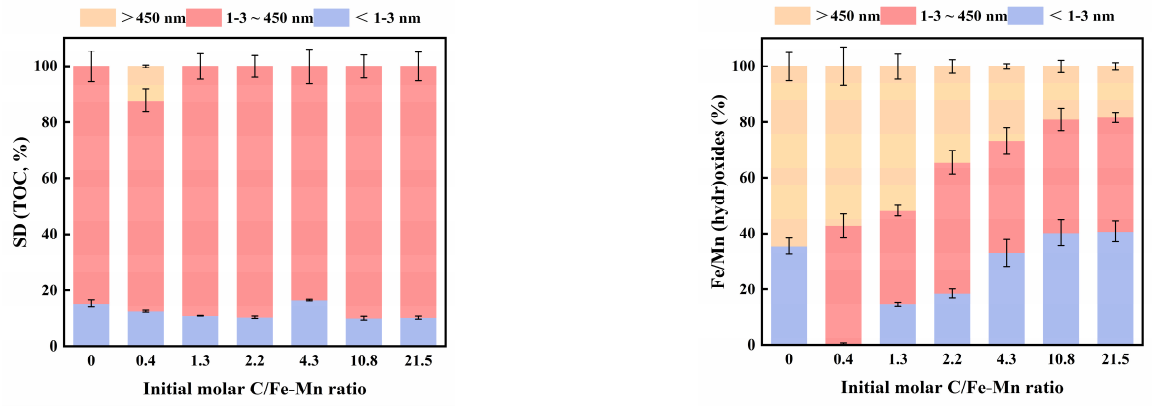

Figure 3. Particle size distribution of (**a**) SD, (**b**) Fe/Mn (hydr)oxides in SD-Fe/Mn suspensions with varying C/Fe-Mn molar ratios.

Further, the relationship between the morphology of Fe/Mn (hydr)oxides and the C/Fe-Mn molar ratio was examined, as illustrated in Figure 3b. It can be observed that, as the C/Fe-Mn molar ratio increases from 0.4, the percentage of particulate Fe/Mn (hydr)oxides (>450 nm) decreases. In contrast, the percentages of colloidal particles (ranging from 1–3 nm to 450 nm) and dissolved species (<1–3 nm) exhibit a corresponding increase in their proportions of Fe/Mn (hydr)oxides. At a C/Fe-Mn ratio of 2.2, the proportion of colloidal Fe/Mn (hydr)oxides reaches a maximum value of 47.1%. Beyond this ratio, the percentage of colloidal Fe/Mn (hydr)oxides stabilizes at approximately 40.0%,

while the concentration of dissolved species continues to increase. Since there exists a direct correlation between the increase in the C/Fe-Mn molar ratio and the concentration of SD, it can be inferred that the rise in the proportion of dissolved species at C/Fe-Mn ratios exceeding 2.2 is likely due to the interaction between organic acids present in SD and Fe/Mn (hydr)oxides. This interaction subsequently influences both the structure and morphology of these Fe/Mn (hydr)oxides. With a moderate increase in SD concentration, the complexation becomes more pronounced, resulting in a higher percentage of colloidal particles. However, the sustained elevation of SD leads to an increased presence of Fe/Mn (hydr)oxides in the dissolved state rather than facilitating their transition into a colloidal form. Therefore, the content of SD plays a crucial role in regulating the formation of Fe/Mn colloids.

The impact of varying concentrations of SD on colloid formation was investigated by analyzing the changes in zeta potential at the colloid surface. The results are presented in Figure 4a. At a C/Fe-Mn molar ratio of 0, the surface of the Fe/Mn (hydr)oxides exhibits a weak negative charge. The electronegativity of the SD-Fe/Mn colloidal surface was markedly enhanced through the continuous introduction of SD and an increase in its organic carbon content. The observed phenomenon can primarily be attributed to the presence of a substantial number of functional groups within the SD molecular structure (Figure S3), including carboxylic acid groups (-COOH) and phenolic hydroxyl groups (-OH) [37,38]. This observation pertains to the presence of complex amino acids and protein-like substances in the two fluorescent components identified through EEM spectroscopy, as well as the predominant functional groups found in aromatic proteins. These functional groups are readily ionizable, allowing for the formation of negative charges under natural conditions. The increased negative surface charge effectively diminishes inter-particle aggregation by means of electrostatic repulsion, consequently leading to a reduction in the formation of particulate matter [39].

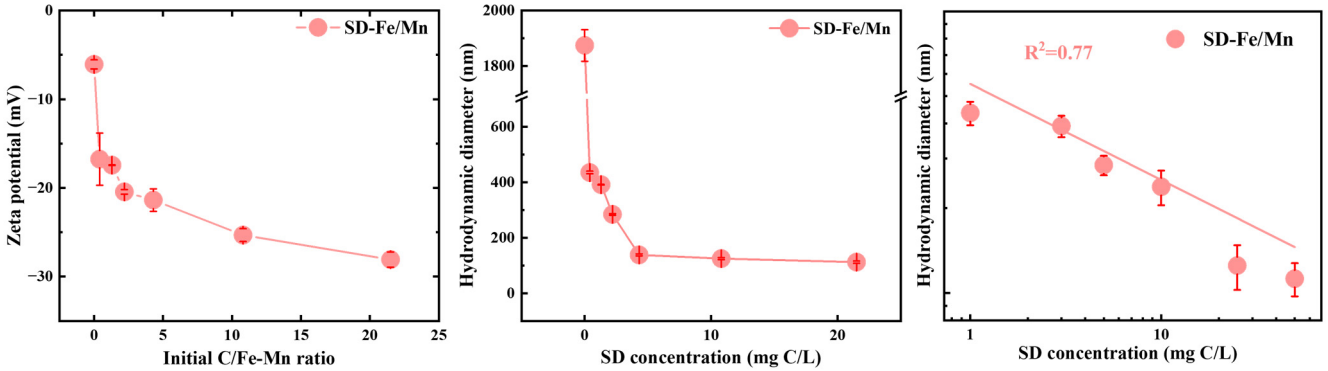

(**a**) (**b**) (**c**)

Figure 4. Relationship between (**a**) Zeta potential, (**b**) particle size, and (**c**) particle size and SD concentration of SD-Fe/Mn colloids with different C/Fe-Mn molar ratios.

The particle size variation in Fe/Mn (hydr)oxides was examined using the dynamic light scattering technique, and the results are presented in Figure 4b. Initially, Fe/Mn (hydr)oxides predominantly existed as large agglomerates with a size of approximately 1900 nm. The particle size stabilizes at around 138.3 nm when the C/Fe-Mn ratio is set to 4.3, and it further decreases to approximately 112.4 nm when the C/Fe-Mn ratio reaches 21.5. These findings are consistent with the morphological distribution results, which indicate that the reduction in particulate matter is attributed to the presence of smaller particle sizes. The relationship between SD concentration and the size of SD-Fe/Mn colloid particles was further investigated, with the results presented in Figure 4c. A weak correlation (R^2 = 0.77) is observed between SD concentration and colloid particle size, suggesting that the interactions between SD and Fe/Mn (hydr)oxides involve complex reaction pathways,

including mechanisms such as complexation and bridging, in addition to electrostatic repulsion [29].

The DLS observations were further validated by characterizing the TEM images of SD-Fe/Mn suspensions, with the results presented in Figure 5. It is evident that a significant number of agglomerates formed from Fe/Mn (hydr)oxides at a C/Fe-Mn molar ratio of 0 (Figure 5a). At a C/Fe-Mn molar ratio of 2.2, flaky SD-Fe/Mn particles were observed, exhibiting an average diameter of approximately 30 nm (Figure 5b). Moreover, as the initial C/Fe-Mn molar ratio increased to 4.3 and subsequently to 21.5, the particle diameters decreased to within the range of 10–30 nm (Figure 5c,d). These morphological changes align well with the DLS results.

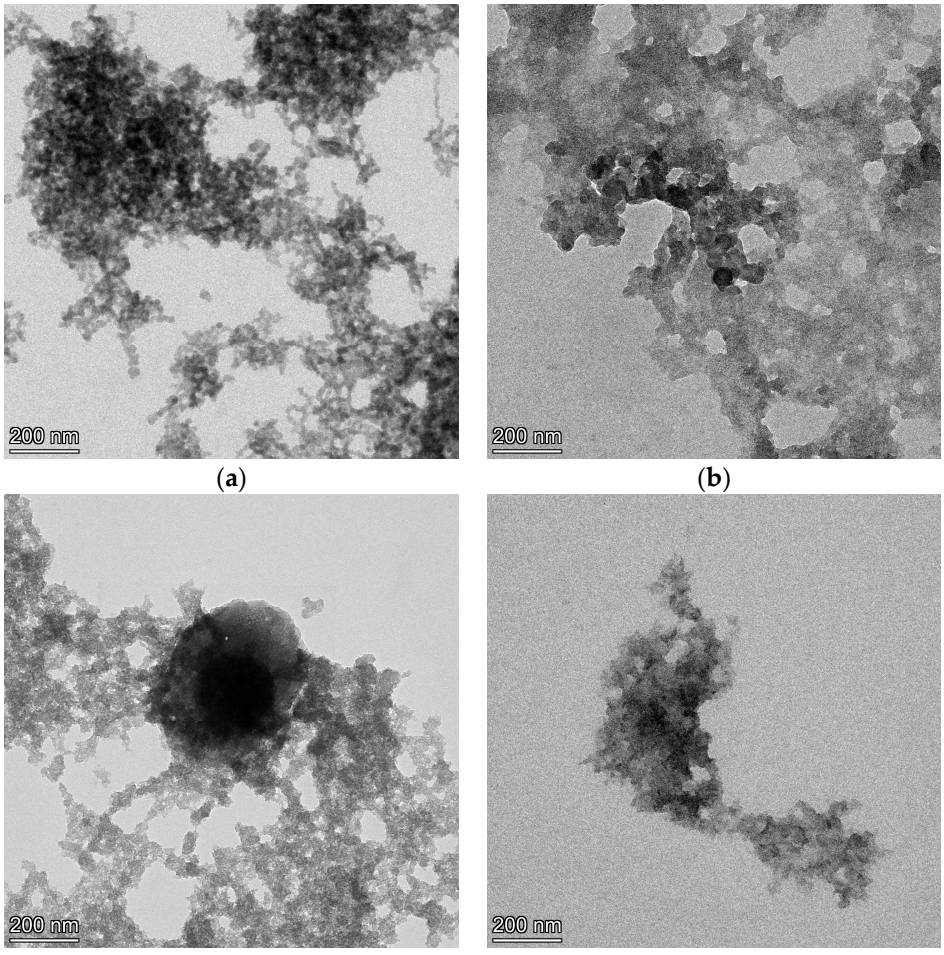

Figure 5. TEM observation of different initial C/Fe-Mn molar ratio suspension: (**a**) C/Fe-Mn = 0, (**b**) C/Fe-Mn = 2.2, (**c**) C/Fe-Mn = 4.3, and (**d**) C/Fe-Mn = 21.5.

3.2. Migration of SD-Fe/Mn Colloids

The migration process of SD-Fe/Mn colloids in soil was simulated using quartz sand-filled columns. The influence of varying C/Fe-Mn molar ratios on the migration behavior of colloidal materials was investigated, with results presented in Figure 6. The penetration curves illustrate the relationship between the initial inflow concentration (C_0) and the effluent concentration (C) of Fe/Mn (hydr)oxides in SD-Fe/Mn suspensions as a function of colloid injection volume (Pore Volume, PV). The infiltration of Fe/Mn (hydr)oxides into SD-Fe/Mn suspensions increased with an elevated C/Fe-Mn molar ratio. At a C/Fe-Mn ratio of 0.4 (1 mg C/L), the SD-Fe/Mn suspension demonstrated minimal penetration through the quartz sand column, achieving a penetration rate of only 3%. Consequently, approximately 97% of the Fe/Mn (hydr)oxides were retained by the quartz sand medium.

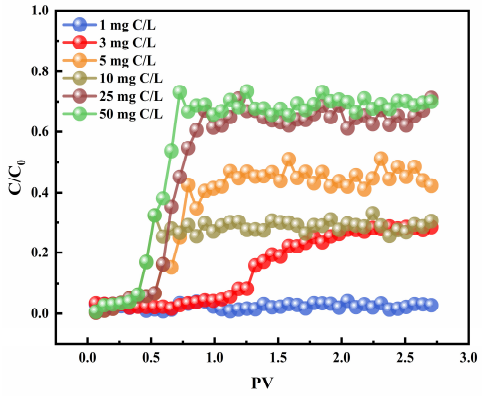

Figure 6. Penetration curves of Fe/Mn (hydr)oxides in SD-Fe/Mn colloids with different C/Fe-Mn molar ratios in columns.

As the C/Fe-Mn molar ratios increased to 1.3 (3 mg C/L) and 2.2 (5 mg C/L), a significant enhancement in penetration rates was observed, reaching values of 28.6% and 30.5%, respectively. An analysis of the distribution patterns for Fe/Mn (hydr)oxides and their fractions within SD-Fe/Mn suspensions indicates that this increase in penetration rate can be attributed to a reduction in particulate fraction, alongside increases in both colloidal particles and dissolved species fractions. The maximum recorded penetration value for Fe/Mn (hydr)oxides within SD-Fe/Mn suspensions was found to be 71.1% at a C/Fe-Mn molar ratio of 21.5 (50 mg C/L). Notably, only approximately 29% of these nanoparticles were retained by the quartz sand media, suggesting that surfactant dispersion significantly enhanced both mobility and transport efficiency for Fe/Mn (hydr)oxides through soil, as influenced by increasing levels of the C/Fe-Mn molar ratio.

3.3. Deposition of SD-Fe/Mn Colloids

To investigate the deposition behavior of SD-Fe/Mn in soil, a silica sensor was employed to simulate the colloidal migration environment. The in situ deposition process of the SD-Fe/Mn suspension onto the silica sensor was continuously monitored in real time using QCM-D (Figure 7). The deposition attachment efficiency (α_D) of SD-Fe/Mn on the silica surface indicates that it exhibits a lower α_D when the C/Fe-Mn molar ratio exceeds 2.2, suggesting that its deposition onto the soil surface is inhibited. α_D is influenced by various factors, including the surface charge of the particles, the pH of the solution, ionic strength, and the presence of surface-active substances. In particular, when considering SD-Fe/Mn as a surface-active agent, it has been observed that SD decreases α_D by enhancing the electrostatic repulsive forces among Fe/Mn (hydr)oxides. Electrostatic repulsion inhibits the attachment of negatively charged SD-Fe/Mn to the negatively charged sensor surface in a near-neutral environment (pH 7). This observation aligns with the findings from SD-Fe/Mn migration experiments. At C/Fe-Mn molar ratios exceeding 2.2, the migration of Fe/Mn (hydr)oxides is enhanced, resulting in reduced deposition. Interestingly, the SD-Fe/Mn suspension with a C/Fe-Mn molar ratio of 2.2 exhibits the lowest α_D in the deposition experiments. Generally speaking, lower α_D values are more likely to facilitate migration within quartz sand media. However, the penetration rates observed are lower when compared to SD-Fe/Mn suspensions with C/Fe-Mn molar ratios of 4.3, 10.8, and 21.5. This phenomenon may be attributed to the fact that, in addition to the electrostatic interactions, the binding strength of the SD-Fe/Mn nanoparticles at their interface with silica also influences their migration and deposition within the silica medium [40,41].

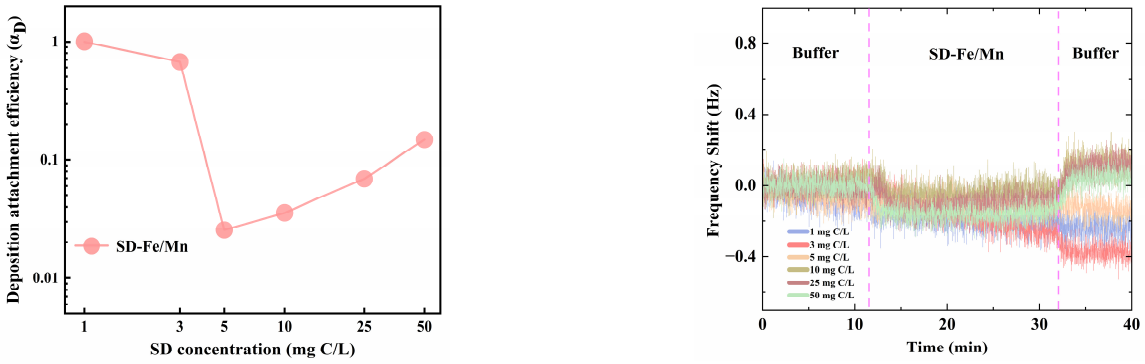

Figure 7. Normalized frequency shifts at the third overtone of (**a**) attachment efficiency of SD–Fe/Mn colloids deposited on the silica surface; (**b**) SD–Fe/Mn colloids deposited on the silica surface.

The time variation curves of the normalized frequency shift for SD-Fe/Mn suspensions were further analyzed, and the results are presented in Figure 5b. It is evident that all samples experienced varying degrees of deposition when the SD-Fe/Mn suspension was introduced into the chamber. The elution experiments conducted after 30 min indicate that when the C/Fe-Mn molar ratio is below 2.2 (5 mg C/L), the deposited layer of SD-Fe/Mn suspension on the silica surface does not desorb in response to the shear force exerted by the water flow of the rinsing solution. It has been demonstrated that SD-Fe/Mn with lower C/Fe-Mn molar ratios (below 2.2) enhances its resistance to shear forces exerted by water flow. This improvement is attributed to the formation of stronger chemical bonds or physical adsorption between the material and the silica surface.

3.4. Effect of SD-Fe/Mn on Arsenic Migration

Based on the aforementioned analyses, a study was conducted to investigate the effects of straw return on the formation, transport, and deposition of Fe/Mn colloids in soil. Furthermore, the impact of formed SD-Fe/Mn colloids on the fate of heavy metal arsenic in soil was examined. Decarbonized extracted bioavailable As (DEB-As) was obtained through carbonate extraction to evaluate arsenic uptake and bioavailability [42,43]. The influence of SD-Fe/Mn colloids on the mobility and potential bioavailability pathways of arsenic within the soil environment was predicted using a combination of soil column experiments and calculations. Quartz sand was utilized to simulate the soil environment and to examine transport processes by constructing soil-filled columns with a comparable porosity of 27.2 $\pm$ 0.2%, similar to those employed in in situ remediation experiments for arsenic in soil [33,35]. Sampling tests were performed at various depths and locations using these soil column experiments (Figure 8h) to assess how SD-Fe/Mn suspensions with distinct C/Fe-Mn molar ratios influenced the migration of heavy metal arsenic within the soil environment, with the results presented in Figure 8. As illustrated in Figure 5a, in soil environments where only straw was incorporated, the average DEB-As content increased by a factor of 1.35 (C/C_0) following multi-point sampling and testing. In contrast, other soil environments treated with SD-Fe/Mn exhibited significantly higher values. This indicates that merely adding straw is ineffective for immobilizing heavy metal As; rather, it markedly elevated DEB-As levels in the soil, thereby enhancing its mobility. This phenomenon may be attributed to complex formation between As and organic acids released during straw decomposition, which increases both solubility and bioavailability. However, for those soil environments where SD-Fe/Mn suspensions were applied, the DEB-As content decreased across soils with varying C/Fe-Mn molar ratios (Figure 8b–g). This suggests that SD-Fe/Mn suspensions effectively inhibited both the migration and bioavailability of As. This phenomenon arises from the ability of arsenic to co-precipitate with Fe/Mn (hydr)oxides, resulting in the formation of new solid compounds. This process effectively

immobilizes arsenic in a solid state, thereby reducing its concentration and mobility within the aqueous phase.

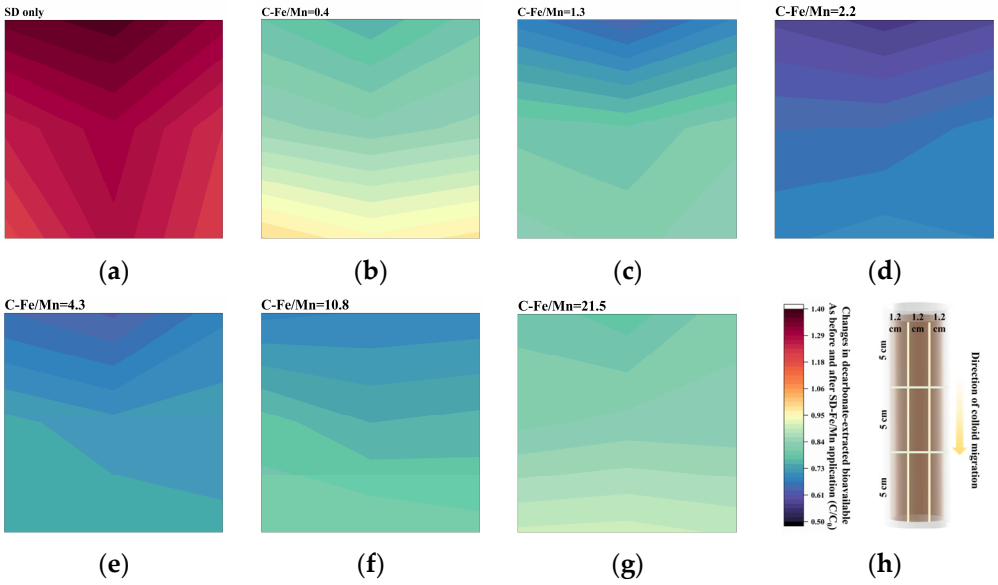

Figure 8. Spatial distribution of the ratio of bioavailable As extracted by carbonate (C) to the initial concentration (C_0) after reaction for 7 days through 1–15 cm soil columns with SD-Fe/Mn colloids at different C/Fe-Mn molar ratios. (**a**) SD only, (**b**) C/Fe-Mn = 0.4, (**c**) C/Fe-Mn = 1.3, (**d**) C/Fe-Mn = 2.2, (**e**) C/Fe-Mn = 4.3, (**f**) C/Fe-Mn = 10.8, (**g**) C/Fe-Mn = 21.5. (**h**) Legend and scale for spatial distribution, where the horizontal 3.5 cm is divided into three sections, and the vertical 15 cm is also divided into three sections.

Further studies demonstrated that the effects of SD-Fe/Mn colloids with varying SD contents on As in the soil were distinct. For SD-Fe/Mn suspensions with C/Fe-Mn molar ratios of 0.4, 1.3, 2.2, 4.3, 10.8, and 21.5, the average DEB-As content in the upper soil layer (0–5 cm) decreased by 26%, 37%, 44%, 38%, 32%, and 24% (C/C_0 for the uppermost layer). Within the range of C/Fe-Mn molar ratios from 0.4 to 2.2, an increase in SD content led to the intensified precipitation of the composite colloid SD-Fe/Mn, which allowed for a greater proportion of components from the SD-Fe/Mn suspension to be retained in the topsoil layer; this effectively hindered the large-scale migration of As.

4. Discussion

This study elucidates the transport mechanisms of SD-Fe/Mn colloids, which are formed from SD and Fe/Mn (hydr)oxides within the rice–soil system. Furthermore, it emphasizes their significant role in mitigating the bioavailability of arsenic. The findings indicate that the molar ratio of C/Fe-Mn significantly influences the morphology of Fe/Mn (hydr)oxides, with higher ratios promoting the formation of colloidal and dissolved forms rather than particulate forms. This transformation is linked to the interaction between SD organic acids and Fe/Mn (hydr)oxides, which modifies their state of existence and solubility. The stability of SD-Fe/Mn complexes increases with higher SD content, indicating that increased negative surface charge reduces aggregation. Zeta potential measurements and DLS analyses confirm that elevated SD concentrations produce smaller, more stable colloidal particles. Combined with the column migration experiments, it is suggested that higher C/Fe-Mn ratios will enhance the fluidity of the SD-Fe/Mn colloid. This enhancement is crucial for effectively managing heavy metal pollutants, such as As, in agricultural soil.

Additionally, QCM-D shows that at greater C/Fe-Mn ratios, the deposition rates of these colloids on silica surfaces decrease. Importantly, the co-precipitation of arsenic with Fe/Mn (hydr)oxides led to the formation of solid compounds that effectively immobilized As, thereby reducing its concentration and mobility in the soil aqueous phase. The incorpo-

ration of SD-Fe/Mn colloids significantly diminished both the mobility and bioavailability of As in the soil. Optimal immobilization occurred at a C/Fe-Mn ratio of 2.2, highlighting the potential application of SD-Fe/Mn colloids in As remediation strategies. These findings emphasize the need to optimize the C/Fe-Mn ratio for effective soil remediation aimed at sustainably reducing As contamination.

5. Conclusions

In this study, we highlight the significant role of the synergy between SD and Fe/Mn (hydr)oxides colloids in mitigating As contamination in agricultural soils. The results indicate that the molar ratio of SD to Fe/Mn (C/Fe-Mn) is a critical factor influencing the formation, stability, and mobility of SD-Fe/Mn colloidal particles. An elevated C/Fe-Mn ratio promotes the formation of colloidal and dissolved Fe/Mn (hydr)oxide species, which interact with SD organic matter, thereby altering their solubility and aggregation. Data from zeta potential assessments, DLS, and QCM-D confirm that an increased content of SD leads to more stable and mobile colloidal particles. This enhancement facilitates the transport and deposition mechanisms of As. The effectiveness of introducing Fe/Mn (hydr)oxides in reducing the mobility and bioavailability of As in soil was validated through indoor soil column experiments. The results indicated that at the optimal C/Fe-Mn ratio of 2.2, both the bioavailability and mobility of As were significantly diminished, thereby effectively preventing the passive uptake of arsenic by plants. These discoveries underscore the importance of fine-tuning the C/Fe-Mn ratio for designing effective and sustainable soil remediation technologies aimed at reducing heavy metal As pollution in soils. They provide assistance in the remediation of heavy metals in agricultural soils, thereby contributing to sustainable development.

Supplementary Materials: The following supporting information can be downloaded at: https://www.mdpi.com/article/10.3390/met14111289/s1. Figure S1: Concentration gradient experiment for SD; Figure S2: Three-dimensional fluorescence EEM of SD; Figure S3. FTIR results of SD–Fe/Mn; Table S1: Soil physical and chemical properties; Table S2: Summary of batch SD-Fe/Mn colloids formation experiments.

Author Contributions: Conceptualization, J.Z. and W.Y.; formal analysis, J.Z., M.S. and Q.L. (Qingzhu Li); methodology, J.Z., Z.Y. and W.Y.; writ-ing—original draft, M.J., Z.Y., Q.L. (Qi Liao) and W.Y.; writing—review and editing, J.Z., M.J., Q.L. (Qingzhu Li), Z.Y., Q.L. (Qi Liao), M.S. and W.Y. All authors have read and agreed to the published version of the manuscript.

Funding: This work was supported by National Natural Science Foundation of China (U23A20679), Key Research and Development Project of the Power Construction Corporation of China (No. DJ-ZDXM-2023-24), Hunan Provincial Natural Science Foundation (2023JJ0065, 20230106ST).

Data Availability Statement: The original contributions presented in the study are included in the article; further inquiries can be directed to the corresponding author (yang220@csu.edu.cn).

Conflicts of Interest: The authors declare no conflicts of interest.

References

1. Zhou, J.; Chen, L.H.; Peng, L.; Luo, S.; Zeng, Q.R. Phytoremediation of heavy metals under an oil crop rotation and treatment of biochar from contaminated biomass for safe use. *Chemosphere* **2020**, *247*, 125856. [CrossRef] [PubMed]
2. Singh, S.; Yadav, R.; Sharma, S.; Singh, A.N. Arsenic contamination in the food chain: A threat to food security and human health. *J. Appl. Biol. Biotechnol.* **2023**, *11*, 24–33. [CrossRef]
3. Yi, K.; Fan, W.; Chen, J.; Jiang, S.; Huang, S.; Peng, L.; Zeng, Q.; Luo, S. Annual input and output fluxes of heavy metals to paddy fields in four types of contaminated areas in Hunan Province, China. *Sci. Total Environ.* **2018**, *634*, 67–76. [CrossRef] [PubMed]
4. Moulick, D.; Samanta, S.; Sarkar, S.; Mukherjee, A.; Pattnaik, B.K.; Saha, S.; Awasthi, J.P.; Bhowmick, S.; Ghosh, D.; Samal, A.C.; et al. Arsenic contamination, impact and mitigation strategies in rice agro-environment: An inclusive insight. *Sci. Total Environ.* **2021**, *800*, 149477. [CrossRef]
5. Zhu, Y.; Williams, P.N.; Meharg, A.A. Exposure to inorganic arsenic from rice: A global health issue? *Environ. Pollut.* **2008**, *154*, 169–171. [CrossRef]

6. Zhang, X.; Zhang, P.; Wei, X.; Peng, H.; Hu, L.; Zhu, X. Migration, transformation of arsenic, and pollution controlling strategies in paddy soil-rice system: A comprehensive review. *Sci. Total Environ.* **2024**, *951*, 175500. [CrossRef]
7. Kapaj, S.; Peterson, H.; Liber, K.; Bhattacharya, P. Human health effects from chronic arsenic poisoning—A review. *J. Environ. Sci. Heal. Part A* **2006**, *41*, 2399–2428. [CrossRef]
8. Abdul, K.S.M.; Jayasinghe, S.S.; Chandana, E.P.S.; Jayasumana, C.; De Silva, P.M.C.S. Arsenic and human health effects: A review. *Environ. Toxicol. Pharmacol.* **2015**, *40*, 828–846. [CrossRef]
9. Liu, C.; Lu, M.; Cui, J.; Li, B.; Fang, C. Effects of straw carbon input on carbon dynamics in agricultural soils: A meta-analysis. *Glob. Chang. Biol.* **2014**, *20*, 1366–1381. [CrossRef]
10. Zhao, J.-Y.; Ye, Z.-H.; Zhong, H. Rice root exudates affect microbial methylmercury production in paddy soils. *Environ. Pollut.* **2018**, *242*, 1921–1929. [CrossRef]
11. Khan, S.; Wu, Y.; Zhang, X.; Hu, S.; Li, T.; Fu, Y.; Li, Q. Influence of dissolved organic matter from corn straw on Zn and cusorption to Chinese loess. *Toxicol. Environ. Chem.* **2013**, *95*, 1318–1327. [CrossRef]
12. McLaughlin, M.J.; Zarcinas, B.A.; Stevens, D.P.; Cook, N. Soil testing for heavy metals. *Commun. Soil Sci. Plant Anal.* **2000**, *31*, 1661–1700. [CrossRef]
13. Bauer, M.; Blodau, C. Mobilization of arsenic by dissolved organic matter from iron oxides, soils and sediments. *Sci. Total Environ.* **2006**, *354*, 179–190. [CrossRef] [PubMed]
14. Abdelrady, A.; Sharma, S.; Sefelnasr, A.; Kennedy, M. Characterisation of the impact of dissolved organic matter on iron, manganese, and arsenic mobilisation during bank filtration. *J. Environ. Manag.* **2020**, *258*, 110003. [CrossRef]
15. Bauer, M.; Blodau, C. Arsenic distribution in the dissolved, colloidal and particulate size fraction of experimental solutions rich in dissolved organic matter and ferric iron. *Geochim. Cosmochim. Acta* **2009**, *73*, 529–542. [CrossRef]
16. Xu, P.; Sun, C.; Ye, X.; Xiao, W.; Zhang, Q.; Wang, Q. The effect of biochar and crop straws on heavy metal bioavailability and plant accumulation in a Cd and Pb polluted soil. *Ecotoxicol. Environ. Saf.* **2016**, *132*, 94–100. [CrossRef]
17. Chen, X.; He, H.; Chen, G.; Li, H. Effects of biochar and crop straws on the bioavailability of cadmium in contaminated soil. *Sci. Rep.* **2020**, *10*, 9528. [CrossRef]
18. Jin, S.; Huang, Y.; Dong, C.; Bai, Y.; Pan, H.; Hu, Z. Effects of different straw returning amounts and fertilizer conditions on bacteria of rice's different part in rare earth mining area. *Sci. Rep.* **2023**, *13*, 412. [CrossRef]
19. Cui, J.; Jing, C. A review of arsenic interfacial geochemistry in groundwater and the role of organic matter. *Ecotoxicol. Environ. Saf.* **2019**, *183*, 109550. [CrossRef]
20. Adusei-Gyamfi, J.; Ouddane, B.; Rietveld, L.; Cornard, J.; Criquet, J. Natural organic matter-cations complexation and its impact on water treatment: A critical review. *Water Res.* **2019**, *160*, 130–147. [CrossRef]
21. Åström, M.; Corin, N. Abundance, sources and speciation of trace elements in humus-rich streams affected by Acid sulphate soils. *Aquat. Geochem.* **2000**, *6*, 367–383. [CrossRef]
22. Haque, S.E.; Tang, J.; Bounds, W.J.; Burdige, D.J.; Johannesson, K.H. Arsenic geochemistry of the great dismal swamp, virginia, USA: Possible organic matter controls. *Aquat. Geochem.* **2007**, *13*, 289–308. [CrossRef]
23. Li, Q.; Xie, L.; Jiang, Y.; Fortner, J.D.; Yu, K.; Liao, P.; Liu, C. Formation and stability of NOM-Mn(III) colloids in aquatic environments. *Water Res.* **2019**, *149*, 190–201. [CrossRef]
24. Liao, P.; Li, W.; Jiang, Y.; Wu, J.; Yuan, S.; Fortner, J.D.; Giammar, D.E. Formation, aggregation, and deposition dynamics of NOM-Iron colloids at anoxic–oxic Interfaces. *Environ. Sci. Technol.* **2017**, *51*, 12235–12245. [CrossRef]
25. Faixo, S.; Gehin, N.; Balayssac, S.; Gilard, V.; Mazeghrane, S.; Haddad, M.; Gaval, G.; Paul, E.; Garrigues, J.-C. Current trends and advances in analytical techniques for the characterization and quantification of biologically recalcitrant organic species in sludge and wastewater: A review. *Anal. Chim. Acta* **2021**, *1152*, 338284. [CrossRef]
26. Wen, L.; Xuan, L.; Chunxiao, H.; Li, G.; Haiming, W.; Ming, L. A new view into three-dimensional excitation-emission matrix fluorescence spectroscopy for dissolved organic matter. *Sci. Total Environ.* **2023**, *855*, 158963. [CrossRef]
27. Zheng, J.; Xie, Y.; Ping, Y.; Xu, H.; Li, Q.; Liao, Q.; Li, Q.; Yang, Z.; Yang, W.; Si, M. Crystal phase conversion of amorphous Fe-Mn binary oxides promote the sequestration and redistribution of arsenic, cadmium, and lead in the soil: Comparison with crystalline form. *J. Environ. Chem. Eng.* **2024**, *12*, 113342. [CrossRef]
28. Zhang, Y.; Zhang, N.; Qian, A.; Yu, C.; Zhang, P.; Yuan, S. Effect of C/Fe Molar Ratio on H_2O_2 and •OH Production during Oxygenation of Fe(II)-Humic Acid Coexisting Systems. *Environ. Sci. Technol.* **2022**, *56*, 13408–13418. [CrossRef]
29. Jeewani, P.H.; Ling, L.; Fu, Y.; Van Zwieten, L.; Zhu, Z.; Ge, T.; Guggenberger, G.; Luo, Y.; Xu, J. The stoichiometric C-Fe ratio regulates glucose mineralization and stabilization via microbial processes. *Geoderma* **2021**, *383*, 114769. [CrossRef]
30. Li, H.; Santos, F.; Butler, K.; Herndon, E. A critical review on the multiple roles of manganese in stabilizing and destabilizing soil organic matter. *Environ. Sci. Technol.* **2021**, *55*, 12136–12152. [CrossRef]
31. Zheng, J.; Jiang, M.; Li, Q.; Yang, W. The formation and stability of HA–Fe/Mn colloids in saturated porous media. *Environments* **2024**, *11*, 136. [CrossRef]
32. Yan, M.; Liu, C.; Wang, D.; Ni, J.; Cheng, J. Characterization of adsorption of humic acid onto alumina using quartz crystal microbalance with dissipation. *Langmuir* **2011**, *27*, 9860–9865. [CrossRef] [PubMed]
33. Chen, Q.; Xu, S.; Liu, Q.; Masliyah, J.; Xu, Z. QCM-D study of nanoparticle interactions. *Adv. Colloid Interface Sci.* **2016**, *233*, 94–114. [CrossRef] [PubMed]

34. Yan, X.; Fei, Y.; Yang, X.; Liang, T.; Zhong, L. Enhanced delivery of engineered Fe-Mn binary oxides in heterogeneous porous media for efficient arsenic stabilization. *J. Hazard. Mater.* **2022**, *424*, 127371. [CrossRef] [PubMed]
35. Ren, Z.; Gui, X.; Xu, X.; Zhao, L.; Qiu, H.; Cao, X. Microplastics in the soil-groundwater environment: Aging, migration, and co-transport of contaminants—A critical review. *J. Hazard. Mater.* **2021**, *419*, 126455. [CrossRef]
36. Sun, P.; Shijirbaatar, A.; Fang, J.; Owens, G.; Lin, D.; Zhang, K. Distinguishable transport behavior of zinc oxide nanoparticles in silica sand and soil columns. *Sci. Total Environ.* **2015**, *505*, 189–198. [CrossRef]
37. Grossl, P.R.; Inskeep, W.P. Characterization of the hydrophobic acid fraction isolated from a wheat straw extract. *Soil Sci. Soc. Am. J.* **1996**, *60*, 158–162. [CrossRef]
38. Lapierre, C. Determining lignin structure by chemical degradations. In *Lignin and Lignans: Advances in Chemistry*; CRC Press: Boca Raton, FL, USA, 2010; pp. 11–48.
39. Heil, D.; Sposito, G. Organic matter role in illitic soil colloids flocculation: II. Surface charge. *Soil Sci. Soc. Am. J.* **1993**, *57*, 1246–1253. [CrossRef]
40. Fatisson, J.; Domingos, R.F.; Wilkinson, K.J.; Tufenkji, N. Deposition of TiO_2 nanoparticles onto silica measured using a quartz crystal microbalance with dissipation monitoring. *Langmuir* **2009**, *25*, 6062–6069. [CrossRef]
41. Arab, D.; Pourafshary, P. Nanoparticles-assisted surface charge modification of the porous medium to treat colloidal particles migration induced by low salinity water flooding. *Colloids Surf. A Physicochem. Eng. Asp.* **2013**, *436*, 803–814. [CrossRef]
42. Liao, Q.; He, L.; Tu, G.; Yang, Z.; Yang, W.; Tang, J.; Cao, W.; Wang, H. Simultaneous immobilization of Pb, Cd and As in soil by hybrid iron-, sulfate-and phosphate-based bio-nanocomposite: Effectiveness, long-term stability and bioavailablity/bioaccessibility evaluation. *Chemosphere* **2021**, *266*, 128960. [CrossRef]
43. Umair, M.; Zafar, S.H.; Cheema, M.; Usman, M. New insights into the environmental application of hybrid nanoparticles in metal contaminated agroecosystem: A review. *J. Environ. Manag.* **2024**, *349*, 119553. [CrossRef]